CLUSIM: A synthetic aperture radar clutter simulator for planetary exploration.

Ya. A. Ilyushin,[1,2] R. Orosei,[3] O. Witasse,[4] and B. Sanchez-Cano,[5]

[1] Atmospheric Physics Department,

Physical Faculty, Moscow State University,

GSP-2, Lengory Moscow 119992, Russia,

phone 007-495-939-3252

ilyushin@phys.msu.ru, rx3ahl@mail.ru

[2] Institute of Radio-engineering and

Electronics, ulitza Mokhovaya, 11/7 Moscow

125009 Russia phone 007 (495) 629-35-74

[3] Istituto di Radioastronomia, Istituto

Nazionale di Astrofisica, Via Piero Gobetti

101, 40129, Bologna, Italy

roberto.orosei@inaf.it

[4]European Space Agency Keplerlaan 2200

AG Noordwijk The Netherlands

owitasse@cosmos.esa.int

[5]Radio and Space Plasma Physics Group,

Department of Physics and Astronomy,

University of Leicester, University Road,

Leicester LE1 7RH, United Kingdom.

bscmdr1@leicester.ac.uk

Key Points.

- ◦ The clutter simulating program CLUSIM is developed and described in details
- ◦ Proposed clutter simulation approach is applicable to both vector and scalar wave fields
- ◦ Proposed approach is free of the Bragg diffractional artifacts caused by rectangular facet models
- ◦ **Ionospheric phase distortion correction procedure is robust with respect to the surface clutter.**

Abstract. In this paper we present the CLUtter SIMulator (CLUSIM), a special program simulating radar side echoes from rough planetary surfaces using realistic topography data sets. A numerical model of realistic topography of the Martian surface, based on Mars Orbiter Laser Altimeter data, is developed. A specially developed computer routine for evaluation of wide band radar echoes reflected from rough surfaces, capable of aperture synthesis simulation, is described. A synthetic radargram for a portion of Mars Express (MEX) orbit 9466 is computed and validated against experimental data obtained by the MARSIS radar instrument. Finally, a previously developed ionospheric phase correction procedure is numerically tested with new simulated echo signals. **Impact of the surface clutter on the ionospheric correction procedure is investigated with a direct numerical comparison to a known benchmark result, which shows robustness of the correction algorithm with respect to the surface clutter.**

1. Introduction.

Ground Penetrating Radar (GPR) is a well-established geophysical technique employed for more than five decades to investigate the terrestrial subsurface. It is based on the transmission of radar pulses in the medium, in high and very high frequency (MF, HF and VHF, respectively) portions of the electromagnetic spectrum into the surface, to detect reflected signals from subsurface structures (see e.g. [*Bogorodsky et al.*, 1985]). Orbital GPR experiments (Figure 1) have been successfully employed in planetary exploration in Mars and in the Moon [*Phillips and et al.*, 1973; *Picardi*, 2004; *Seu et al.*, 2007; *Ono et al.*, 2009], and are often called subsurface radar sounders. Recently, two GPR instruments, Radar for Europa Assessment and Sounding: Ocean to Near-surface (REASON) [*Pettinelli et al.*, 2015] and Radar for Icy Moon Exploration (RIME) [*Bruzzone et al.*, 2013], have been selected for the interplanetary missions Europa Clipper [*Phillips and Pappalardo*, 2014] and JUICE [*Grasset et al.*, 2013], respectively.

Another instrument, the bistatic radar sounder Comet Nucleus Sounding Experiment by Radiowave Transmission (CONSERT) onboard the ROSETTA space mission [*Kofman et al.*, 1998; *Herique et al.*, 1999] has revealed the difference of electrical properties of mantle and core of the cometary nucleus [*Ciarletti et al.*, 2015], which has been first theoretically investigated by *Ilyushin et al.* [2003]; *Ilyushin and Kunitsyn* [2008]. Recently, passive radar instruments [*Romero-Wolf et al.*, 2015; *Hartogh and Ilyushin*, 2016; *Schroeder et al.*, 2016] using radio noise emissions of Jupiter as a signal for radio probing Jovian icy moons were also discussed.

By detecting dielectric discontinuities associated with compositional and/or structural discontinuities, radar sounders are the only remote sensing instruments suitable for the study of the deep subsurface of a planet from orbit.

However, planetary landscapes are typically rough. The radar signal is therefore contaminated by undesirable echoes, which mask useful subsurface reflections and should be filtered out from the radar data. Thus, this clutter should be taken into account during the radar data processing. In fact, the first successful GPR experiment on Apollo-17 lunar-orbiting mission [*Peeples et al.*, 1978] revealed the need for context images of the sub-satellite landscape for visual identification of echo-producing surface features. In Mars Advanced Radar for Subsurface and Ionosphere Sounding (MARSIS) radar experiment on board Mars Express (MEX) spacecraft, dual antenna clutter cancelation scheme has been implemented [*Picardi, G., et al.*, 1999; *Jordan et al.*, 2009]. A monopole antenna, with zero gain in the nadir direction, recieves side clutter only. This was then subtracted from the main dipole antenna signal. However, complete elimination of the clutter echoes is not yet possible.. More sophisticated radar techniques, such as focused aperture synthesis, synthetic aperture radar (SAR) interferometry etc., which require much higher data transfer and processing rates, might be a solution of this problem in future. Now, surface clutter can be simulated, compared to real experiment data and subtracted from it more or less accurately. Thus, numerical simulation of the clutter is a necessary stage of the radar data analysis and interpretation procedure [*Nunes et al.*, 2010, 2011].

Theoretical clutter estimates are also required at all the stages of the radar experiment, including instrument design and observational strategy planning. For these purposes, one needs a radar experiment model, allowing for these estimates. This model in turn should consist of the physical model of the object structure (surface) and algorithm for the numerical solution of the electromagnetic equations, ruling an interaction of the electromagnetic wave with the object.

Development of SAR clutter simulation tool, capable of high resolution topographic data assimilation, and efficiently exploiting powerful resources of modern computing machinery available now, for the Martian applications is the motivation of this investigation.

The paper is organized as follows. The new clutter simulator CLUSIM, which is the main goal of this study, is described in the Section 2 (the Martian surface topography model and the algorithm for the electromagnetic scattering simulation in the Subsections 2.1 and 2.2, respectively). Section 3 is entirely devoted to the ionospheric correction algorithm test, including the Martian ionospheric model and phase correction approach. Simulation results are validated against the experimentally measured data from the MARSIS instrument and briefly discussed in the Section 5, and in the Section 6 the conlusions are formulated and some final remarks are given.

2. Synthetic aperture radar clutter simulator.

Clutter simulators [*Spagnuolo et al.*, 2011; *Russo et al.*, 2008; *Nouvel et al.*, 2004] consist of two basic structure units: a topography interpolator and a radar echo simulator itself.

Both the rough surface model and the approach to the electromagnetic equations itself can be deterministic or statistical. To validate the detection of subsurface interfaces, numerical electromagnetic models of surface scattering should be used to produce simulations of surface echoes, which are then compared to real echoes detected by the radar. A realistic model of the surface should be based on real observations.

Accounting for these considerations, a special package of computer codes named CLUSIM (CLUtter SIMulator) has been developed and tested by us for the Mars case. The package consists of the topography analyzer and numerical integration routine. Topography analyser block in turn includes routines for Mars Orbiter Laser Altimeter (MOLA) data assimilation, their preprocessing and preselection, removal of suspicious (non-reliable) data, topography interpolation and visual control.

The main purpose of the package is the simulation of radargrams at any given part of the spacecraft orbit.

2.1. Topography interpolation

Historically, topographic datasets suitable for the simulation of surface electromagnetic scattering in planetary exploration have been obtained through remote sensing techniques, such as laser altimetry [*Smith et al.*, 2001, 2010], microwave radar altimetry (e.g. [*Ford and Pettengill*, 1992]), photogrammetry (e.g. [*Jaumann et al.*, 2007; *Kirk et al.*, 2008; *Preusker et al.*, 2011]) and photoclinometry (e.g. [*Kirk et al.*, 2003]).

For Mars, the MOLA database is probably the most used and best developed source of surface topography data. These data are available in the form of structured list of latitudes, longitudes and heights of the MOLA spots grouped in orbital tracks. The spatial resolution of these data is about 300 m along a track, and up to several kilometers across it from track to track [*Smith et al.*, 2001]. To build a Digital Elevation Model (DEM), which is an importan part of the clutter simulating algorithm, these data must be interpolated on the planetary surface, giving the surface height as a function of latitude and longitude.

To do this, the following approach is applied. All the available MOLA spots are projected on the tangent plane to the subsatellite point of the planetary surface, keeping their ordered track structure. After that, the height profile along each track is approximated by a cubic spline. Then, a regular grid of parallel lines is built on the tangent surface plane. This grid also considers the grid lines of the height profile, which are defined by the MOLA tracks in the crossing points. Again, this is approximated by a cubic spline. Finally, an uniform spaced rectangular grid is built on these grid lines, which gives an approximation of the rough surface terrain. Accuracy of this approximation in a given point of the surface should be on the order of height difference between adjacent MOLA spots nearest to this given point. On the MOLA spots, this approximation exactly corresponds to the MOLA surface elevation data. Thus the surface topography is defined as a function of Cartesian coordinates on the tangent plane. The curvature of the spherical surface (deviations of the spherical surface from the tangent plane) can be now just added to the topography approximation, if necessary. In practice, the impact of the planetary surface curvature is small, so the tangent plane approximations yields the satisfactory results.

With that approximate topography defined on the tangent plane with Cartesian coordinates, one can evaluate the numerical solution of the electromagnetic problem of interaction of the sounding wave with the object of known shape.

2.2. Algorithms for solving electromagnetic field equations.

An approach to the numerical solving of the electromagnetic waves equations can also be deterministic [*Fa and Jin*, 2010; *Liu et al.*, 2014] or statistical [*Ilyushin*, 2014]. In the deterministic case of an object of a given structure, there are no principal difficulties to numerically solve electrodynamical equations. A number of algorithms, such as Finite Difference in Time Domain (FDTD) [*Yee*, 1966], Finite Element Method (FEM) [*Zienkiewicz et al.*, 2013], Discrete Dipole Approximation (DDA) [*Purcell and Pennypacker*, 1973], T-matrix [*Waterman*, 1965] etc., are well developed now.

However, planetary radar echo simulations are characterized by a large object size (compared to the wavelength) and by a wide frequency spectrum of the signal. Strict approaches of the computational electrodynamics mentioned above (FEM,FDTD,DDA etc.), are in fact inapplicable to this particular case of the SAR sounding of the planetary surface because of the large size of the object. The known reported FDTD-simulations are one- or two-dimensional [*Xu et al.*, 2006] or restricted to a little domain of the medium [*Boisson et al.*, 2009]. Application of the aperture synthesis and other averaging signal processing techniques, such as migration [*Herique and Kofman*, 1997], requires their adequate representation in the numerical model, which in turn results in many repeated calculations of the same type with different input parameters, and the computation load is vastly increased. Estimates of mean signal parameters, averaged over many realizations, result in additional increase of computational complexity. Probably for this reason, most known clutter simulations are more or less simplified, e.g. lack the aperture synthesis [*Smirnov et al.*, 2014; *Fa and Jin*, 2010]. In other simulation algorithms, the aperture synthesis is performed at the post-processing stages [*Berquin et al.*, 2015].

Thus, for such problems of scattering from the large rough surfaces, approximate techniques are more appropriate. Since the height profile is not small compared to the wavelength, the small perturbation technique is also not appropriate. The only feasible approach is Kirchhoff approximation [*Beckmann and Spizzichino*, 1963; *Ogilvy*, 1991], which is typically used to solve these kind of problems. Making use of the vectorial Huygens-Fresnel principle, which is a counterpart for the conventional scalar Kirchoff approximation, allows one to consider polarization of the radar echoes and depolarizing effects. However, depolarization is known to be absent within the gently undulating surface approximation [*Beckmann and Spizzichino*, 1963; *Ogilvy*, 1991], which is a reasonable assumption for many planetary terrains. On the other hand, much depolarization of the reflected waves comes from the discrete objects and small scale structures, which available DEM of planetary surfaces do not account for.

It is worth mentioning here that given the wavelength of the MARSIS carrier signals, the presence of rocks, even if they were several decimeters in length, is unlikely to significantly effect the echo signal. *Neumann et al.* [2003] estimated the roughness of the Martian surface within the MOLA footprint (75 m across) from the widening of the pulse echo. They found that, over the vast majority of the Martian surface, the root mean square (rms) height of the surface is at most a few meters. Notable exceptions are the Olympus Mons areole and the Olympia Undae dune field. However, for much of the Martian surface, the small-scale roughness height is a very small fraction of the MARSIS wavelength, which ranges between 60 and 170 m.

In addition, a single reflection from a rough surface-to-vacuum interface, typical for the terrestrial planets, does not produce high reflection amplitude nor significant change of the wave polarization state in the experimental planetary radar studies [*Hagfors*, 1967; *Black et al.*, 2001a]. Both anomalously high radar albedo and strong depolarization of radar pulses are typical for galilean satellites of Jupiter [*Ostro and Shoemaker*, 1990]. These remarkable properties of the Jovian icy moons have been attributed to the volume scattering [*Hagfors et al.*, 1997], multiple subsurface reflections [*Eshleman*, 1986; *Ostro and Pettengill*, 1978] and coherent backscattering enhancement effect [*Black et al.*, 2001b; *Hapke*, 1990; *Hapke and Blewett*, 1991]. Since both volume scattering and coherent backscattering enhancement are not expected in the Martian crust at MARSIS wavelengths, we do not include these effects in our model model. These effects are discussed in [*Ilyushin*, 2012]. In our present study, we neglect the polarization of the waves and restrict our consideration to the conventional scalar Kirchhoff approximation. As it has been shown by *Ilyushin* [2014], the calculation of the reflected radar signal spectrum (complex surface reflection coefficient $R(\omega)$) within this approximation reduces to the numerical evaluation of the Kirchhoff integral over the whole reflecting surface

$$R(\omega) = \int G(\mathbf{r_0}, \mathbf{r})\, G(\mathbf{r}, \mathbf{r_0})\, exp(-2ikh(x, y))\, dx\, dy\,, \tag{1}$$

where $\mathbf{r_0}(\mathbf{t})$ and $\mathbf{r}$ are the source (spacecraft) location point and surface point of integration, respectively, and $h(x, y)$ is the local surface height.

The Green function of the Helmholtz equation in the paraxial approximation equals to

$$G(\mathbf{r}, \mathbf{r}') = \frac{k}{2\pi i|z - z'|} \exp\left(ik|z - z'| + ik\frac{(x - x')^2}{2|z - z'|} + ik\frac{(y - y')^2}{2|z - z'|}\right)\,, \tag{2}$$

where $k = \omega/c$ [*Goodman*, 1996].

For a dielectric surface with finite permittivity, this expression should be multiplied by the Fresnel reflection coefficient R_F. Due to the near-nadir sounding geometry of the orbital GPR instruments and moderate slopes typical for much of the Martian surface, the Fresnel reflection for normal incidence is a reasonable approximation

$$R_F = \frac{\sqrt{\varepsilon} - 1}{\sqrt{\varepsilon} + 1}\,, \tag{3}$$

where ε is a permittivity of the surface. Here we assume that the surface is homogeneous and its permittivity is uniform everywhere.

In the Kirchhoff approximation, the complex amplitude of the radar echo depends on the dielectric permittivity only through this coefficient (3). Since the primary objective of our simulations is the ratio of the main nadir echo to the side clutter echoes rather than signal-to-noise-ratio (SNR), we do not pursue the absolute signal level calibration here and simply assume $R_F = 1$ everywhere, which corresponds to an ideal reflective surface.

If the aperture synthesis is applied, an extra integration over the spacecraft coordinate is needed (see Fig. 1). **Aperture synthesis is essentially averaging over a portion of a satellite trajectory of length $2L$ (synthetic aperture) with a weighting function $\exp\left(\frac{2\pi i s\nu}{2L}\right)$, where s is the coordinate along the trajectory, ν is the Doppler filter number (positive or negative integer). In this paper we consider only the most important case $\nu = 0$.**

Averaging the Eq. (1) over the synthetic aperture, we obtain

$$\frac{1}{2L}\int_{-L}^{L} R(\omega)dx_0 = \frac{k^{3/2}\sqrt[4]{-1}}{8L\pi^{3/2}z^2}\int e^{ik\frac{y^2}{2z}+2ikz-2ikh(x,y)}\left(erf\left(\frac{1}{2}(-1)^{3/4}\sqrt{k}(L-x)\right)+erf\left(\frac{1}{2}(-1)^{3/4}\sqrt{k}(L+x)\right)\right)d^2\mathbf{r}\,, \tag{4}$$

assuming that satellite trajectory $\mathbf{r_0(t)} = \{x_0(t), 0, z\}$ is parallel to the x axis and the horizontal. Small deviations from a horizontal trajectory can be easily accounted for in the phase exponent in (4). Integrals of the quadratic exponent involved here, resulting in the error function of complex argument in the Eq. (4), can be effectively expressed through the so-called Faddeeva function [*Abramowitz and Stegun*, 1972]. Recently, a computer code package in C++ and Fortran languages has been released by *Johnson* [2012]. With it, all the computations can be implemented on modern high-performance computing machines.

For the piecewise-planar approximation of the surface elevation with triangular of rectangular facets, the complex reflectance of an individual facet $R_f(\omega)$ can be derived from (4) as follows (see the Figure 2)

$$R_f(\omega) = \int dy \int\limits_{x_1(y)}^{x_2(y)} dx \frac{1}{2L} \int\limits_{-L}^{L} R(\omega) dx_0 \,, \tag{5}$$

where $x_1(y)$ and $x_2(y)$ are the left and right boundaries of the given facet. The inner integration (over the x variable) can be performed analytically over the triangular of rectangular facet (see [*Ilyushin*, 2004]). Total echo signal from the whole rough surface is therefore a sum of contributions of all the facets $R_f(\omega)$, all of which is an one-fold integral in spatial domain.

Berquin et al. [2015] make use of the vectorial Huygens-Fresnel principle and derive an expression for polarized radar echo from the planetary surface

$$\mathbf{E}_s(\mathbf{x}_0, \omega) = \int ik\bar{\bar{\mathbf{G}}}(\mathbf{x}_0, \mathbf{x}, \omega) \Big(\eta \left[\hat{\mathbf{n}} \times \mathbf{H}\right](\mathbf{x}, \omega) + \hat{\mathbf{k}}_s \times \left[\hat{\mathbf{n}} \times \mathbf{E}\right](\mathbf{x}, \omega)\Big) \, d\sigma(\mathbf{x}) \tag{6}$$

with the dyadic Green function

$$\bar{\bar{\mathbf{G}}}(\mathbf{x}_0, \mathbf{x}, \omega) = \left[\bar{\bar{\mathbf{I}}} - \hat{\mathbf{k}}_s \hat{\mathbf{k}}_s\right] \frac{e^{ik|\mathbf{x}-\mathbf{x}_0|}}{4\pi |\mathbf{x} - \mathbf{x}_0|} \,, \tag{7}$$

where $\mathbf{E}$ and $\mathbf{H}$ denote electric and magnetic fields, respectively, $\hat{\mathbf{n}}$ is a unit normal to the surface, $\mathbf{x}$ is a point on the surface, $\eta = \sqrt{\mu/\varepsilon}$ is the characteristic impedance of the surface, ε and μ are the permittivity and permeability, k is the wave number and $\hat{\mathbf{k}}_s$ is the unit vector pointing in the scattering direction. Assuming the length of the synthetic aperture to be small compared to the spacecraft orbit height, we can regard $\hat{\mathbf{k}}_s$ as a constant and integrate over the synthetic aperture analytically, as is explained above for the scalar case. However, if the gently undulating surface approximation is adopted, there are no depolarization of the radar echoes [*Beckmann and Spizzichino*, 1963; *Ogilvy*, 1991]. On scales well exceeding the sounding wavelengths, for which the Kirchhoff approximation and Huygens-Fresnel principle are valid, most Martian terrain can be regarded as smooth gently undulating surfaces [*Kreslavsky, M.A. and J.W. Head III*, 2000]. The radar echo can be more or less depolarized by the surface features (rocks, boulders etc.) comparable with the wavelength. However, because planetary GPR instruments have not yet had polarimetric capabilities, for purely energetic assessments we perform our numerical simulations within the conventional scalar Kirchhoff approximation.

Berquin et al. [2015] also derive an expression for the diffraction integral over the whole surface of the triangular facet as an approximate sum of an infinite series. These approximate expressions cannot be further integrated analytically, so the aperture synthesis can only be performed numerically on the post-processing stage. In addition to complicated procedure of adding up many terms of the sum, the approximation error results in spurious reflections coming from the edges of the facets, in turn causing the Bragg diffraction maxima produced even by the perfectly flat surface approximated by such facets. To remove this, *Berquin et al.* [2015] proposed to use irregular grids for the facet approximation. Our approach with analytical aperture synthesis is free of these Bragg diffractional artifacts, and provides more flexibility in the choice of DEM, since it is not confined to the constant phase and linear phase approximations of the surface. The aperture synthesis approach which is proposed here, can also be applied to the case of vector field simulation. The exponent in the (7) is expanded in series in small variations of the spacecraft coordinate $\mathbf{x}_0$ and integrated over, yielding the expression containing the error function like (4) as well as in the scalar case. After that, further integration over the rough surface can be performed using different approaches, thus avoiding emulation of the aperture synthesis at the post-processing stage.

When the radar echo spectrum is evaluated, the signal can be obtained with standard signal processing technique (matched filtration). An expression for the compressed radar signal $s(t)$ with partial correction of the ionospheric phase distortions [*Ilyushin and Kunitsyn*, 2004] writes

$$s(t) = \frac{1}{2\pi} \int\limits_{-\infty}^{+\infty} H(\omega) F^*(\omega) F(\omega) R(\omega) \exp(-i\omega t + \phi(\omega) - \tilde{\phi}(\omega)) d\omega \,, \tag{8}$$

$$\phi(\omega) = 2k \int\limits_0^z n(z) dz, \tag{9}$$

$$n(z) = \sqrt{1 - \frac{\omega_p^2(z)}{\omega^2}} \,, \tag{10}$$

$$\omega_p^2(z) = 4\pi r_e N(z) c^2 = \frac{N(z) e^2}{m_e \epsilon_0}, \tag{11}$$

where $\omega = 2\pi f$ is the angular frequency, $k = \frac{\omega}{c}$ is the wave number, $H(\omega)$ is the spectral window function, $F(\omega)$ is initial radar pulse spectrum radiated by an instrument, $R(\omega)$ is a complex reflection coefficient of rough surface, $n(z)$ - height profile of the ionospheric refractive index, $\omega_p(z)$ is angular plasma frequency, $N(z)$ is ionospheric plasma electron concentration, r_e is classical electron radius, and c is light speed in vacuum. Natural ionospheric phase shift $\phi(\omega)$ is adaptively compensated by the phase curve $\tilde{\phi}(\omega)$ [*Ilyushin and Kunitsyn*, 2004]. As a compensating phase term, a phase curve $\phi(\omega)$ of artificially constructed model plasma layer with negative sign is often used. *Ilyushin and Kunitsyn* [2004] analyzed a wide set of radio occultation profiles of Martian ionosphere available at that time and found that the triangular vertical profile of plasma density distribution is optimal for compensating phase distortions occurring in real Martian ionosphere.

Further radar signal processing methods (migration etc.) can be then applied to the simulated signals if necessary. As it has been shown by *Ilyushin* [2010, 2009a], radar wave scattering due to the plasma frequency fluctuations is relatively weak, except of specific ionospheric situations (high plasma frequency and intense fluctuations during strong solar events). *Safaeinili et al.* [2003] studied not only ionospheric phase distortion, but also impact of the effect of Faraday rotation of wave polarization plane. They showed that in weak local magnetic fields, typical for Mars, this effect is not pronounced and may be neglected, even in measurements with polarization-sensitive antennas. Thus in most situations, the ionosphere can be regarded as a flat layered slab of an isotropic dispersive medium. Under assumed approximations the ionospheric phase delay $\phi(\omega)$ and the phase correction term $\tilde{\phi}(\omega)$ are represented by separate factors and can thus be considered independently in the simulations. We omit it everywhere, except in the section describing a test of ionospheric correction algorithm with newly simulated clutter data.

Practical success of this numerical approach therefore depends on the quality of the surface height approximation, discretization of the integral sum and approximation of the integrands by analytical expressions. [*Nouvel et al.*, 2004] adopted rectangular facet approximation of the rough surface. Such an approximation results in an analytical representation of the Kirchhoff integral over a single facet. Summing contributions of all the facets, one gets the complex amplitude of the monochromatic wave, reflected from the whole surface. If the facet edges are properly oriented (parallel and perpendicular to the spacecraft trajectory), integration along this trajectory (aperture synthesis) can also be performed analytically, yielding a result expressed through the Fresnel integrals in closed form.

In some specific cases, practical realization of facet approach is rather effective and physically adequate. *Ilyushin* [2004] adopted a piecewise-planar approximation of Martian polar trough profile, and simulated MARSIS radar echoes coming from these troughs for different mutual orientation of the polar troughs and spacecraft trajectory. Essentially the one-dimensional character of the valley allowed for continuous piecewise linear profile, ensuring high simulation accuracy at reasonable computational expenses. It has been shown by [*Ilyushin*, 2004] that for proper (normal) mutual orientation of the orbit and the trough, surface clutter generated by the trough is well suppressed by aperture synthesis (practically, below the dynamic range of the radar sounder).

However, the rectangular plane tile (facet) approximation of arbitrary 3D rough surface is, generally speaking, discontinuous (Fig. 3). Such discontinuities of the model surface should generate artifacts, contaminating the result with unphysical reflections.

Continuous approximations are more complicated. The simplest one is the triangulation (planar approximation on the triangular grid, Fig. 4). Surface triangulation has been used for clutter simulation in some radar studies [*Fa and Jin*, 2010; *Liu et al.*, 2014], however, aperture synthesis technique was not applied there. To do this, one has to average the complex reflection amplitude (1) over some portion of the satellite trajectory.

Diffraction integral in Eq. (1) over the triangular domain cannot be expressed in closed analytical form. However, integration over the spacecraft trajectory can be analytically performed. Thus, evaluation of the signal spectrum reduces to the numerical estimate of the Kirchhoff diffraction integral (1) over the whole surface with the integration kernel (4). The compressed radar pulse in time domain can then be evaluated by common matched filtration technique. We used the same pulse compression procedure as in our previous studies, where this procedure is described in detail by [*Ilyushin*, 2004, 2008, 2009b]. Systematic phase shift, introduced by the ionosphere, can be introduced separately as an independent exponential factor at the signal compression stage.

The structure of the clutter simulation algorithm is shown in the flowchart (Fig. 5). Raw topographic data, obtained from the MOLA data archive (stage I), are interpolated along each track (stage II) and then across the tracks (stage III). For each point of the orbit, where the sounding with a sequence of chirp pulses (synthetic aperture) is performed, the interpolated topographic data are triangulated on the regular grid centered around the subsatellite point (stage IV). After that, the complex reflection coefficient of the rough surface (4) is evaluated (stage V) by the integration over the surface for each of the discrete frequencies, constituting the digital representation of the radar signal spectrum, in the cycle (stage VI). In the simulation 512 frequencies are used, as well as in the current MARSIS experiment.

After that, the signal is evaluated from its spectrum with the Fast Fourier Transform (FFT) procedure (stage VII), using common matched filtration procedure with Hann spectral window [*Harris*, 1978], according to the MARSIS technical specifications [*Picardi, G., et al.*, 1999; *Picardi, G. et al.*, 2001]. The signals are routinely calculated for a number of points along the MEX

spacecraft orbit (stage VIII, cycle) for which the measured signal records are available. All the signals are then assembled into the radargram (stage IX, final), characterizing radar clutter echoes coming from the surface terrain on the given portion of the planetary surface landscape. The radargram is then represented graphically in the standard way.

3. Ionospheric model and correction algorithm tests.

As planetary atmospheres are ionized by solar radiation, they become a dispersive medium for relatively long radar waves, used in subsurface sounding. The radar signals become distorted by the ionospheric phase dispersion [*Safaeinili et al.*, 2003; *Cartacci et al.*, 2013; *Sanchez-Cano et al.*, 2015]. The radar data processing routine must therefore include some special procedure for extra phase shift compensation [*Armand and Smirnov*, 2003; *Ilyushin and Kunitsyn*, 2004; *Mouginot et al.*, 2008], adaptive or not. Impact of random wave scattering on the function of these algorithms have been previously studied [*Ilyushin*, 2008; *Ilyushin et al.*, 2012]. In this study, we perform a numerical test of the previously developed phase compensation algorithm [*Ilyushin and Kunitsyn*, 2004] together with a realistic surface clutter model. The reader is referred to [*Ilyushin and Kunitsyn*, 2004] for the detail description of the ionospheric correction approach tested here.

For these simulations, we use a new developed empirical model for the dayside electron density of the martian ionosphere (primary and secondary layer), called NeMars [*Sanchez-Cano et al.*, 2013]. The model is largely based on MARSIS Active Ionospheric Sounding (AIS) mode data [*Gurnett et al.*, 2005a; *Morgan et al.*, 2013; *Sánchez-Cano et al.*, 2012] and to a lesser extent on radio occultation data from the Mars Global Surveyor mission.

In addition, this model partially assumes the Chapman theory. This model reproduces to a reasonable degree the main characteristics of the vertical electron density profiles obtained with the two techniques by considering solar zenith angle, solar flux F10.7 as a proxy of the solar activity, and heliocentric distance. Typical model profiles used for the present simulation are shown in the Figure 6.

For testing purposed, a special MARSIS radargram with adaptive compensation of model ionospheric distortions was simulated. As a source of initial ionospheric distortions, the NeMars model has been used. For the adaptive compensation of the distortion, a phase curve of a plasma slab layer with triangular height profile of the electron density [*Ilyushin and Kunitsyn*, 2004]

$$\omega_p^2(z) = \omega_c^2(z)(1 - (z - z_0)/H)\,, 0 < z - z_0 < H\,, \tag{12}$$

has been used. Partial phase distortion is mitigated by adjusting the phase curve of the correcting plasma layer close to real ionospheric phase curve, which is unknown, and subtracting it from the signal phase. In practice, the parameters of correcting plasma layer (plasma critical frequency ω_c^2 and ionospheric layer thickness H) have been adjusted for optimal (maximal) intensity contrast [*Ilyushin and Kunitsyn*, 2004]

$$C_I^2 = \frac{\frac{1}{\tau}\int\limits_{t_0}^{t_1} |s(t)|^4 dt - \left(\frac{1}{\tau}\int\limits_{t_0}^{t_1} |s(t)|^2 dt\right)^2}{\left(\frac{1}{\tau}\int\limits_{t_0}^{t_1} |s(t)|^2 dt\right)^2}\,. \tag{13}$$

In this work, the adaptive ionospheric phase correction is performed on the post processing stage, after the matched filtration. However, within the paraxial approximation adopted by us phase and clutter responses are multiplicative and can therefore be evaluated independently.

4. Results of numerical simulations.

We present here sample results obtained for the southmost portion of MEX 9466 orbit. MOLA topography of the surface landscape surrounding the subsatellite track and its visual image provided by the High Resolution Stereo Camera (HRSC) [*Neukum and Jaumann*, 2004] are shown in the Figures 7 and 8, respectively.

Figure 9 consists of five panels, each of them represents a measures or simulated radargram. Each radargram shows the intensity of radar echo in gray shades against echo signal delay (vertical axis) and position of the spacecraft in the orbit (horizontal axis) in the standard way typically used for radar data representation. Simulated radargrams are shown in the Figure 9, panel b-e**, together with the experimental MARSIS radargram (the Figure 9, panel** a**).**

The radargrams presented in this paper represent about 118 s of observations at an altitude of 390 km and a speed of 4.2 km/s. MARSIS transmitted a linearly-modulated, 350 s-long pulse (a ”chirp”) that can be centered at 1.8, 3, 4 or 5 MHz, with a 1 MHz bandwidth. In the observations considered in this paper, the central frequency of the chirp was 5 MHz. The pulse echo is down-converted to a central frequency of 0.7 MHz, and sampled by the analog-to-digital converter at 2.8 MHz sampling rate. In-phase and quadrature components (I/Q) synthesis then reduces the sampling rate at 1.4 MHz. The synthetic aperture length $2L$ **during observations ranged from 2016 to 2226 m. In the simulation, the value** $2L = 2500\,m$ **was used, which is close to optimal value for the unfocused aperture synthesis (half Fresnel zone size** $\sqrt{\lambda z}/2 = 2100\,m$**).**

For the assessment of the aperture synthesis efficiency, a single pulse radar sounder echo has been simulated (shown in the Figure 10 together with the synthetic aperture echo, for comparison). Namely, solid and dotted curves in the Figure 10 represent radar signals with the application of the aperture synthesis and without it.

Finally, to comparatively investigate complexity of ionospheric compensation with ideally flat and realistic rough surface, we show the plots of intensity contrast C_I^2 (13) of simulated radar signals with partial compensation of the ionospheric phase distortion. The graphs of the contrast calculated for the reflection from ideally flat surface and realistic martian surface terrain are shown in the Figures 11 and 12, respectively. There is shown dependence of the contrast function C_I^2 on the two leading terms of the Taylor series of phase mismatch $\phi(\omega) - \tilde{\phi}(\omega)$ in (8), i.e. $a_2(\omega - \omega_0)^2$ and $a_3(\omega - \omega_0)^3$, where ω_0 is the central angular frequency of the radar chirp band.

5. Discussion of the numerical results.

Numerically simulated results are in good agreement both with measured data and theoretical predictions.

While the experimental radargram (panel *a* was computed from real radar pulses distorted by the ionospheric phase dispersion, and therefore was corrected for it, in the simulated radargram shown on the panel *b* ionospheric phase shifts were not taken in account. To demonstrate the ionospheric correction algorithm performance, the results of simulations with accounting for ionospheric frequency dispersion of the phase and its partial correction is presented in the Fig. 9 separately (panel *d*). It can be seen that the simulated results match the measurements with a reasonable degree of agreement.

Some inaccuracies may arise from intrinsic errors of the Kirchhoff approximation applied here for the electromagnetic wave scattering description. On the other hand, they may occur due to some object features (variable material properties etc.), completely missing in our simple model of perfectly reflecting surface of a given shape.

Ionospheric distortions, being properly compensated, also do not significantly impact the final result (the Fig. 9, panel *e*). To show how much distortion was in fact caused by the ionosphere in MEX orbit 9466, simulated radargram uncorrected for the ionospheric distortions is also shown in the Figure 9 (panel *c*).

The ionospheric parameters chosen for the simulations correspond to the true conditions of the Martian atmosphere, which took place during the MEX 9466 orbit measurements. This orbit crosses the solar terminator in its northern part, and in ist southern part, which is analyzed here, the solar zenith angle changed within a range from 61 to 66 degrees. According to radio occultation measurements [*Zhang et al.*, 1990] and MARSIS results [*Gurnett et al.*, 2005b], the maximal plasma frequency of the Martian ionosphere exceeds 3.5 MHz for the solar zenith angles (SZA) smaller than 50°, approaching 4 MHz at $SZA < 40°$ and exceeding this value during solar events. The NeMars ionospheric model predicts the maximal plasma frequency values about $f_p \approx 3.4\,MHz$ and $f_p = 4.14\,MHz$ for the $SZA = 60°$ and $SZA = 0°$, respectively. Thus, to make a complete test of the ionospheric correction algorithm performance, we investigate a hypothetical worst case scenario with $SZA = 0°$ (the sun is all the time at the local zenith). Simulated radargram, corresponding to this scenario, is shown in the Fig. 9, panel *v*. One can see notable degradation of the radargram quality, however, it is still readable and interpretable.

Effectiveness of the aperture synthesis largely agrees with theoretical estimates. It can be seen in the Figure 10 that the aperture synthesis is able to suppress side clutter by 15-25 dB. Strong echo at $t = 100\,\mu s$ delay probably comes from transversal direction, which is not suppressed by the aperture synthesis.

The problem of correction of systematic phase distortion and random scattering of the radar signal acting simultaneously, has once been investigated for the diffraction on the ionospheric irregularities by [*Ilyushin*, 2008]. From the algorithmic point of view, the problem effectively reduces to the finding of the correction phase $\tilde{\phi}(\omega)$, corresponding to the maximal value of the function being optimized (i.e. intensity contrast). Under plausible assumptions about the ionospheric irregularities structure, it has been shown that when random scattering is present, the peak of the contrast function C_I^2 is slightly flattened and widened, but still remains unique and unambiguous. So, as a conclusion, random scattering does not significantly complicate the elimination of systematic regular phase distortion in the radar signal. However, no realistic model of kilometer scale irregularities in the Martian ionosphere is know. Due to that, simplified assumptions have been made in that study.

The results of the present investigation largely agree with that previous study. As one can see from these two figures 11 and 12, both graphs demonstrate a clear unique maximum of the contrast function. In the case of realistic surface roughness model, the maximum is somewhat lower and wider than for ideally flat surface, however it can still be easily found algorithmically with standard optimization routines. Thus, the phase correction algorithm based

on the contrast optimization principle proves to be stable and robust with respect to the surface clutter, as well as to the ionospheric random scattering.

6. Conclusions and remarks.

In the paper presented here, a clutter simulating program CLUSIM, capable of emulating realistic radar echoes coming from rough planetary surface, is developed and described in detail. A model of surface landscape topography, based on interpolation of Mars Orbiter Laser Altimeter data set, has been elaborated. Surface echo simulator, exploiting Kirchhoff approximation and capable of simulation of aperture synthesis, developed as a C++ programming language procedure suitable for parallel computing systems using OpenMP parallel programming standard. A sample synthetic radargram is computed and compared to realistic radar instrument data obtained by the MARSIS experiment on board Mars Express interplanetary space mission. Previously elaborated routine for ionospheric distortion correction is also tested with simulated radar echo together with vertical plasma density profiles provided by NeMars ionospheric model, build with data recorded with the other mode of the MARSIS radar. **Comparative numerical tests confirmed the robustness of the ionospheric phase distortion correction algorithm with respect to the surface clutter.**

Acknowledgments.

This work was supported by ESA-ESTEC Faculty and the Italian Space Agency (ASI) through contract no. I/032/12/1. Support from Russian Fundamental Research Fund with the grant 15-02-05476 and Russian National Fund with the grant 17-77-20087 is also kindly acknowledged.

B.S.-C. acknowledges support through STFC grants ST/K001000/1 and ST/N000749/1.

Y.I. is grateful to the administration of the Scientific Research Computing Center of the Moscow State University for granting the access to the computational resources of the parallel computing systems SKIF-GRID "Tchshebyshev" and "Lomonosov".

Authors thank all the reviewers of this paper for constructive reviews and valuable comments. The authors also thank Henrik Melin and Padraig Donnelly for their useful comments. MARSIS subsurface sounding data can be accessed through the Planetary Science Archive of ESA (*https://www.cosmos.esa.int/web/psa/mars-express*) or the PDS Geosciences Node of NASA (*http://pds-geosciences.wustl.edu/missions/mars_express/marsis.htm*). Laser altimetry data from MOLA instrument are available from the archive *http://pds-geosciences.wustl.edu/missions/mgs/mola.html*. Requests for any other data should be sent directly to the corresponding author (Ya.I) ilyushin@phys.msu.ru

References

Abramowitz, M., and I. A. Stegun (1972), *Handbook of Mathematical Functions with Formulas, Graphs, and Mathematical Tables*, Dover Publications, New York.

Armand, N., and V. Smirnov (2003), Distortion of radar pulses by the martian ionosphere, *Radio Science*, *38*(5), 11/1–11/12.

Beckmann, P., and A. Spizzichino (1963), *The Scattering of Electromagnetic Waves from Rough Surfaces*, Macmillan and Company, New York.

Berquin, Y., A. Herique, W. Kofman, and E. Heggy (2015), Computing low-frequency radar surface echoes for planetary radar using Huygens-Fresnel's principle, *Radio Science*, *50*(10), 1097–1109, doi:10.1002/2015RS005714.

Black, G., D. Campbell, and S. Ostro (2001a), Icy galilean satellites: 70 cm radar results from Arecibo, *Icarus*, *151*(2), 160 – 166, doi:10.1006/icar.2001.6615.

Black, G., D. Campbell, and P. Nicholson (2001b), Icy galilean satellites: Modeling radar reflectivities as a coherent backscatter effect, *Icarus*, *151*(2), 167 – 180, doi: 10.1006/icar.2001.6616.

Bogorodsky, V., C. Bentley, and P. Gudmandsen (1985), *Radioglaciology*, Reidel, Dordrecht.

Boisson, J., E. Heggy, S. M. Clifford, A. Frigeri, J. J. Plaut, W. M. Farrell, N. E. Putzig, G. Picardi, R. Orosei, P. Lognonne, and D. A. Gurnett (2009), Sounding the subsurface of Athabasca Valles using MARSIS radar data: Exploring the volcanic and fluvial hypotheses for the origin of the rafted plate terrain, *Journal of Geophysical Research: Planets*, *114*(E8), doi:10.1029/2008JE003299, e08003.

Bruzzone, L., J. Plaut, G. Alberti, D. Blankenship, F. Bovolo, B. Campbell, A. Ferro, Y. Gim, W. Kofman, G. Komatsu, W. McKinnon, G. Mitri, R. Orosei, G. Patterson, D. Plettemeier, and R. Seu (2013), RIME: Radar for icy moon exploration, *European Planetary Science Congress Abstracts*, *8*, EPSC2013–744–1.

Cartacci, M., E. Amata, A. Cicchetti, R. Noschese, S. Giuppi, B. Langlais, A. Frigeri, R. Orosei, and G. Picardi (2013), Mars ionosphere total electron content analysis from MARSIS subsurface data, *Icarus*, *223*(1), 423 – 437, doi:10.1016/j.icarus.2012.12.011.

Ciarletti, V., A. Levasseur-Regourd, J. Lasue, C. Statz, D. Plettemeier, A. Herique, Y. Rogez, and W. Kofman (2015), Consert suggests a change in local properties of 67p/Churyumov-Gerasimenko's nucleus at depth, *Astronomy and Astrophysics*, *583*, doi:10.1051/0004-6361/201526337.

Eshleman, V. R. (1986), Radar glory from buried craters on icy moons, *Science*, *234* (4776), 587–590, doi:10.1126/science.234.4776.587.

Fa, W., and Y. Jin (2010), Simulation of radar sounder echo from lunar surface and subsurface structure, *Science China Earth Sciences*, *53* (7), 1043–1055, doi:10.1007/s11430-010-3070-8.

Ford, P. G., and G. H. Pettengill (1992), Venus topography and kilometer-scale slopes, *Journal of Geophysical Research: Planets*, *97* (E8), 13,103–13,114, doi:10.1029/92JE01085.

Goodman, J. (1996), *Introduction to Fourier Optics*, 2nd ed., MaGraw-Hill.

Grasset, O., M. Dougherty, A. Coustenis, E. Bunce, C. Erd, D. Titov, M. Blanc, A. Coates, P. Drossart, L. Fletcher, H. Hussmann, R. Jaumann, N. Krupp, J.-P. Lebreton, O. Prieto-Ballesteros, P. Tortora, F. Tosi, and T. V. Hoolst (2013), JUpiter ICy moons explorer (JUICE): An ESA mission to orbit Ganymede and to characterise the Jupiter system, *Planetary and Space Science*, *78*, 1 – 21, doi:10.1016/j.pss.2012.12.002.

Gurnett, D. A., D. L. Kirchner, R. L. Huff, D. D. Morgan, A. M. Persoon, T. F. Averkamp, F. Duru, E. Nielsen, A. Safaeinili, J. J. Plaut, and G. Picardi (2005a), Radar soundings of the ionosphere of Mars, *Science*, *310* (5756), 1929–1933, doi:10.1126/science.1121868.

Gurnett, D. A., D. L. Kirchner, R. L. Huff, D. D. Morgan, A. M. Persoon, T. F. Averkamp, F. Duru, E. Nielsen, A. Safaeinili, J. J. Plaut, , and G. Picardi (2005b), Radar soundings of the ionosphere of Mars, *Science*, *310*, 1929, doi:DOI: 10.1126/science.1121868.

Hagfors, T. (1967), A study of the depolarization of lunar radar echoes, *Radio Science*, *2* (5), 445–465, doi:10.1002/rds196725445.

Hagfors, T., I. Dahlstrom, T. Gold, S.-E. Hamran, and R. Hansen (1997), Refraction scattering in the anomalous reflections from icy surfaces, *Icarus*, *130*(2), 313 – 322, doi:10.1006/icar.1997.5844.

Hapke, B. (1990), Coherent backscatter and the radar characteristics of outer planet satellites, *Icarus*, *88*(2), 407–417, doi:10.1016/0019-1035(90)90091-M.

Hapke, B., and D. Blewett (1991), Coherent backscatter model for the unusual radar reflectivity of icy satellites, *Nature*, *352*(6330), 46–47.

Harris, F. J. (1978), On the use of windows for harmonic analysis with the Discrete Fourier Transform, *Proceedings of the IEEE*, *66*(1), 51–83.

Hartogh, P., and Y. Ilyushin (2016), A passive low frequency instrument for radio wave sounding the subsurface oceans of the Jovian icy moons: An instrument concept, *Planetary and Space Science*, *130*, 30 – 39, doi:10.1016/j.pss.2016.05.008, atmospheres, Magnetospheres and Surfaces of the outer planets, their satellites and ring systems: Part XI .

Herique, A., and W. Kofman (1997), Reconstruction by migration of undersampled 2D signals, *IEEE Transactions on Signal Processing*, *45*(9), 2406.

Herique, A., W. Kofman, T. Hagfors, G. Caudal, and J.-P. Ayanides (1999), A characterization of a comet nucleus interior: inversion of simulated radio frequency data, *Planetary and Space Science*, *47*(6-7), 885 – 904, doi:10.1016/S0032-0633(98)00144-5.

Ilyushin, Y. (2008), Distortions of the ultrawideband signals of deep-sensing radars in an irregular ionosphere, *Journal of Communications Technology and Electronics*, *53*(4), 377–386, doi:10.1134/S1064226908040025.

Ilyushin, Y. (2010), Influence of anisotropic fluctuations of the ionosphere plasma density on deep radio sounding by a ultra wide band radar with synthesized aperture, *Cosmic Research*, *48*(2), 157–164.

Ilyushin, Y., and V. Kunitsyn (2004), Methods for correcting ionosphere distortions of orbital ground-penetrating radar signals, *Journal of Communications Technology and Electronics*, *49*(2), 154–165.

Ilyushin, Y. A. (2004), Martian northern polar cap: Layering and possible implications for radar sounding, *Planetary and Space Science*, *52*(13), 1195 – 1207, doi: 10.1016/j.pss.2004.08.002.

Ilyushin, Y. A. (2009a), Impact of the plasma fluctuations in the martian ionosphere on the performance of the synthetic aperture ground-penetrating radar, *Planetary and Space Science*, *57*(12), 1458 – 1466, doi:10.1016/j.pss.2009.07.005.

Ilyushin, Y. A. (2009b), Influence of the ionospheric plasma density fluctuations on the subsurface sounding of the martian soil by a synthetic aperture radar, *Radiophysics and Quantum Electronics*, *52*(5-6), 332–340.

Ilyushin, Y. A. (2012), Coherent backscattering enhancement in highly anisotropically scattering media: Numerical solution, *Journal of Quantitative Spectroscopy and Radiative Transfer*, *113*(5), 348 – 354, doi:10.1016/j.jqsrt.2011.12.003.

Ilyushin, Y. A. (2014), Subsurface radar location of the putative ocean on Ganymede: Numerical simulation of the surface terrain impact, *Planetary and Space Science*, *92*, 121–126.

Ilyushin, Y. A., and V. E. Kunitsyn (2008), Radio sensing of a cometary nucleus: Possibilities for investigating the surface layer, *Journal of Communications Technology and*

Electronics, *53*(5), 545–549, doi:10.1134/S1064226908050094.

Ilyushin, Y. A., T. Hagfors, and V. E. Kunitsyn (2003), Cometary surface layer properties: Possible approaches to radio sounding retrieval during the consert experiment-numerical simulation and discussion, *Radio Science*, *38*(1), 8/1–8/9, doi:10.1029/2001RS002487.

Ilyushin, Y. A., S. V.M., and Y. O.V. (2012), Deep subsurface radar sounding of rough extraterrestrial terrains: Numerical simulations, *2012 6th International Conference on Ultrawideband and Ultrashort Impulse Signals, UWBUSIS 2012 - Conference Proceedings*, pp. 112–114.

Jaumann, R., G. Neukum, T. Behnke, T. Duxbury, K. Eichentopf, J. Flohrer, S. Gasselt, B. Giese, K. Gwinner, E. Hauber, H. Hoffmann, A. Hoffmeister, U. Kohler, K.-D. Matz, T. McCord, V. Mertens, J. Oberst, R. Pischel, D. Reiss, E. Ress, T. Roatsch, P. Saiger, F. Scholten, G. Schwarz, K. Stephan, and M. Wahlisch (2007), The high-resolution stereo camera (HRSC) experiment on Mars Express: Instrument aspects and experiment conduct from interplanetary cruise through the nominal mission, *Planetary and Space Science*, *55*(78), 928 – 952, doi:10.1016/j.pss.2006.12.003.

Johnson, S. G. (2012). $http://ab-initio.mit.edu/wiki/index.php/Faddeeva\_Package$

Jordan, R., G. Picardi, J. Plaut, K. Wheeler, D. Kirchner, A. Safaeinili, W. Johnson, R. Seu, D. Calabrese, E. Zampolini, A. Cicchetti, R. Huff, D. Gurnett, A. Ivanov, W. Kofman, R. Orosei, T. Thompson, P. Edenhofer, and O. Bombaci (2009), The Mars Express MARSIS sounder instrument, *Planetary and Space Science*, *57*(14–15), 1975 – 1986, doi:10.1016/j.pss.2009.09.016.

Kirk, R. L., E. Howington-Kraus, B. Redding, D. Galuszka, T. M. Hare, B. A. Archinal, L. A. Soderblom, and J. M. Barrett (2003), High-resolution topomapping of candidate

MER landing sites with Mars orbiter camera narrow-angle images, *Journal of Geophysical Research: Planets*, *108*(E12), 8088, doi:10.1029/2003JE002131.

Kirk, R. L., E. Howington-Kraus, M. R. Rosiek, J. A. Anderson, B. A. Archinal, K. J. Becker, D. A. Cook, D. M. Galuszka, P. E. Geissler, T. M. Hare, I. M. Holmberg, L. P. Keszthelyi, B. L. Redding, W. A. Delamere, D. Gallagher, J. D. Chapel, E. M. Eliason, R. King, and A. S. McEwen (2008), Ultrahigh resolution topographic mapping of Mars with mro hirise stereo images: Meter-scale slopes of candidate phoenix landing sites, *Journal of Geophysical Research: Planets*, *113*(E3), doi:10.1029/2007JE003000, e00A24.

Kofman, W., Y. Barbin, J. Klinger, A.-C. Levasseur-Regourd, J.-P. Barriot, A. Herique, T. Hagfors, E. Nielsen, E. Grn, P. Edenhofer, H. Kochan, G. Picardi, R. Seu, J. van Zyl, C. Elachi, J. Melosh, J. Veverka, P. Weissman, L. Svedhem, S. Hamran, and I. Williams (1998), Comet nucleus sounding experiment by radiowave transmission, *Advances in Space Research*, *21*(11), 1589 – 1598, doi:10.1016/S0273-1177(97)00952-6.

Kreslavsky, M.A., and J.W. Head III (2000), Kilometer-scale roughness of Mars: results from MOLA data analysis, *J. Geophys. Res.*, *105*(E11), 26,695–26,711.

Liu, C., H. Ye, and Y.-Q. Jin (2014), Simulation of radar echoes from Mars' surface/subsurface and inversion of surface media parameters, *Radio Science*, *49*(7), 473–484, doi:10.1002/2013RS005367.

Morgan, D., O. Witasse, E. Nielsen, D. Gurnett, F. Duru, and D. Kirchner (2013), The processing of electron density profiles from the Mars Express MARSIS topside sounder, *Radio Science*, *48*(3), 197–207, doi:10.1002/rds.20023.

Mouginot, J., W. Kofman, A. Safaeinili, and A. Herique (2008), Correction of the ionospheric distortion on the MARSIS surface sounding echoes, *Planetary and Space Science*, *56*(7), 917–926.

Neukum, G., and R. Jaumann (2004), *HRSC: the High Resolution Stereo Camera of Mars Express*, 17 - 35 pp., Noordwijk, Netherlands: ESA Publications Division.

Neumann, G. A., J. B. Abshire, O. Aharonson, J. B. Garvin, X. Sun, and M. T. Zuber (2003), Mars orbiter laser altimeter pulse width measurements and footprint-scale roughness, *Geophysical Research Letters*, *30*(11), doi:10.1029/2003GL017048, 1561.

Nouvel, J.-F., A. Herique, W. Kofman, and A. Safaeinili (2004), Radar signal simulation: Surface modeling with the facet method, *Radio Science*, *39*(1), doi:10.1029/2003RS002903.

Nunes, D. C., S. E. Smrekar, A. Safaeinili, J. Holt, R. J. Phillips, R. Seu, and B. Campbell (2010), Examination of gully sites on Mars with the shallow radar, *Journal of Geophysical Research: Planets*, *115*(E10), doi:10.1029/2009JE003509, e10004.

Nunes, D. C., S. E. Smrekar, B. Fisher, J. J. Plaut, J. W. Holt, J. W. Head, S. J. Kadish, and R. J. Phillips (2011), Shallow radar (SHARAD), pedestal craters, and the lost martian layers: Initial assessments, *Journal of Geophysical Research: Planets*, *116*(E4), doi:10.1029/2010JE003690, e04006.

Ogilvy, J. (1991), *Theory of Wave Scattering from Random Rough Surfaces*, Adam Hilger, Bristol.

Ono, T., A. Kumamoto, H. Nakagawa, Y. Yamaguchi, S. Oshigami, A. Yamaji, T. Kobayashi, Y. Kasahara, and H. Oya (2009), Lunar radar sounder observations of subsurface layers under the nearside maria of the Moon, *Science*, *323*(5916), 909–912,

doi:10.1126/science.1165988.
Ostro, S. J., and G. H. Pettengill (1978), Icy craters on the galilean satellites?, *Icarus*, *34*(2), 268 – 279, doi:10.1016/0019-1035(78)90167-7.
Ostro, S. J., and E. M. Shoemaker (1990), The extraordinary radar echoes from Europa, Ganymede, and Callisto: A geological perspective, *Icarus*, *85*(2), 335 – 345, doi:10.1016/0019-1035(90)90121-O.
Peeples, W. J., W. R. Sill, T. W. May, S. H. Ward, R. J. Phillips, R. L. Jordan, E. A. Abbott, and T. J. Killpack (1978), Orbital radar evidence for lunar subsurface layering in maria Serenitatis and Crisium, *Journal of Geophysical Research: Solid Earth*, *83*(B7), 3459–3468, doi:10.1029/JB083iB07p03459.
Pettinelli, E., B. Cosciotti, F. Di Paolo, S. E. Lauro, E. Mattei, R. Orosei, and G. Vannaroni (2015), Dielectric properties of Jovian satellite ice analogs for subsurface radar exploration: A review, *Reviews of Geophysics*, *53*(3), 593–641, doi: 10.1002/2014RG000463.
Phillips, C. B., and R. T. Pappalardo (2014), Europa CLIPPER mission concept: Exploring Jupiter's ocean moon, *Eos, Transactions American Geophysical Union*, *95*(20), 165–167, doi:10.1002/2014EO200002.
Phillips, R. J., and et al. (1973), Apollo lunar sounder experiment, *330*(22), 1–26.
Picardi, G. e. (2004), MARSIS: Mars advanced radar for subsurface and ionosphere sounding, *Mars Express: the scientific payload*, pp. 51–69.
Picardi, G., et al. (1999), Martian advanced radar for subsurface and ionospheric sounding (MARSIS): Models and system analysis, *Tech. Rep. MRS-001/005/99 V.2.0 21/05/1999*, InfoCom Dpt.

Picardi, G. et al. (2001), MARSIS flight user manual, *Tech. Rep. ID-MAR-0008-INF*, InfoCom Dpt.

Preusker, F., J. Oberst, J. W. Head, T. R. Watters, M. S. Robinson, M. T. Zuber, and S. C. Solomon (2011), Stereo topographic models of Mercury after three MESSENGER flybys, *Planetary and Space Science*, *59*(15), 1910 – 1917, doi:10.1016/j.pss.2011.07.005.

Purcell, E. M., and C. R. Pennypacker (1973), Scattering and Absorption of Light by Nonspherical Dielectric Grains, *The Astrophysical Journal*, *186*, 705–714, doi: 10.1086/152538.

Romero-Wolf, A., S. Vance, F. Maiwald, E. Heggy, P. Ries, and K. Liewer (2015), A passive probe for subsurface oceans and liquid water in Jupiter's icy moons, *Icarus*, *248*, 463 – 477, doi:10.1016/j.icarus.2014.10.043.

Russo, F., M. Cutigni, R. Orosei, C. Taddei, R. Seu, D. Biccari, E. Giacomoni, O. Fuga, and E. Flamini (2008), An incoherent simulator for the SHARAD experiment, *Radar Conference*.

Safaeinili, A., W. Kofman, J.-F. Nouvel, A. Herique, and R. Jordan (2003), Impact of Mars ionosphere on orbital radar sounder operation and data processing, *Planetary and Space Science*, *51*(7-8), 505–515, doi:10.1016/S0032-0633(03)00048-5.

Sánchez-Cano, B., O. Witasse, M. Herraiz, S. M. Radicella, J. Bauer, P.-L. Blelly, and G. Rodríguez-Caderot (2012), Retrieval of ionospheric profiles from the Mars Express MARSIS experiment data and comparison with radio occultation data, *Geoscientific Instrumentation, Methods and Data Systems*, *1*(1), 77–84, doi:10.5194/gi-1-77-2012.

Sanchez-Cano, B., S. Radicella, M. Herraiz, O. Witasse, and G. Rodriguez-Caderot (2013), NeMars: An empirical model of the martian dayside ionosphere based on Mars Express

MARSIS data, *Icarus*, *225*(1), 236 – 247, doi:10.1016/j.icarus.2013.03.021.

Sanchez-Cano, B. b., D. Morgan, O. Witasse, S. Radicella, M. f. Herraiz, R. Orosei, M. Cartacci, A. Cicchetti, R. Noschese, W. j. Kofman, C. Grima, J. Mouginot, D. Gurnett, M. Lester, P.-L. Blelly, H. Opgenoorth, and G. Quinsac (2015), Total electron content in the martian atmosphere: A critical assessment of the Mars Express MARSIS data sets, *Journal of Geophysical Research A: Space Physics*, *120*(3), 2166–2182, doi:10.1002/2014JA020630.

Schroeder, D. M., A. Romero-Wolf, L. Carrer, C. Grima, B. A. Campbell, W. Kofman, L. Bruzzone, and D. D. Blankenship (2016), Assessing the potential for passive radio sounding of Europa and Ganymede with RIME and REASON , *Planetary and Space Science*, *134*, pp.52–60, doi:10.1016/j.pss.2016.10.007.

Seu, R., R. J. Phillips, D. Biccari, R. Orosei, A. Masdea, G. Picardi, A. Safaeinili, B. A. Campbell, J. J. Plaut, L. Marinangeli, S. E. Smrekar, and D. C. Nunes (2007), SHARAD sounding radar on the Mars Reconnaissance Orbiter, *Journal of Geophysical Research: Planets*, *112*(E5), doi:10.1029/2006JE002745, e05S05.

Smirnov, V., O. Yushkova, I. Karachevtseva, and I. Nadezhdina (2014), The influence of relief on formation of reflected signals of subsurface sounding radar, *Solar System Research*, *48*(3), 176–181, doi:10.1134/S003809461403006X.

Smith, D. E., M. T. Zuber, H. V. Frey, J. B. Garvin, J. W. Head, D. O. Muhleman, G. H. Pettengill, R. J. Phillips, S. C. Solomon, H. J. Zwally, W. B. Banerdt, T. C. Duxbury, M. P. Golombek, F. G. Lemoine, G. A. Neumann, D. D. Rowlands, O. Aharonson, P. G. Ford, A. B. Ivanov, C. L. Johnson, P. J. McGovern, J. B. Abshire, R. S. Afzal, and X. Sun (2001), Mars Orbiter Laser Altimeter: Experiment summary after the first year of global mapping of Mars, *Journal of Geophysical Research: Planets*, *106*(E10), 23,689–23,722, doi:10.1029/2000JE001364.

Smith, D. E., M. T. Zuber, G. A. Neumann, F. G. Lemoine, E. Mazarico, M. H. Torrence, J. F. McGarry, D. D. Rowlands, J. W. Head, T. H. Duxbury, O. Aharonson, P. G. Lucey, M. S. Robinson, O. S. Barnouin, J. F. Cavanaugh, X. Sun, P. Liiva, D.-d. Mao, J. C. Smith, and A. E. Bartels (2010), Initial observations from the Lunar Orbiter Laser Altimeter (lola), *Geophysical Research Letters*, *37*(18), doi:10.1029/2010GL043751, l18204.

Spagnuolo, M., F. Grings, P. Perna, M. Franco, H. Karszenbaum, and V. Ramos (2011), Multilayer simulations for accurate geological interpretations of SHARAD radargrams, *Planetary and Space Science*, *59*(11-12), 1222–1230, doi:10.1016/j.pss.2010.10.013.

Waterman, P. (1965), Matrix formulation of electromagnetic scattering, *Proceedings of the IEEE*, *53*(8), 805–812, doi:10.1109/PROC.1965.4058.

Xu, Y., S. A. Cummer, and W. M. Farrell (2006), Application of an orbital radar sounder model to detecting martian polar subsurface features, *Journal of Geophysical Research: Planets*, *111*(E6), doi:10.1029/2005JE002547, e06S17.

Yee, K. (1966), Numerical solution of inital boundary value problems involving Maxwell's equations in isotropic media, *Antennas and Propagation, IEEE Transactions on*, *14*(3), 302–307.

Zhang, M. H. G., J. G. Luhmann, and A. J. Kliore (1990), An observational study of the nightside ionospheres of Mars and Venus with radio occultation methods, *J. Geophys. Res.*, *95*, 17,095–17,102, doi:10.1029/JA095iA10p17095.

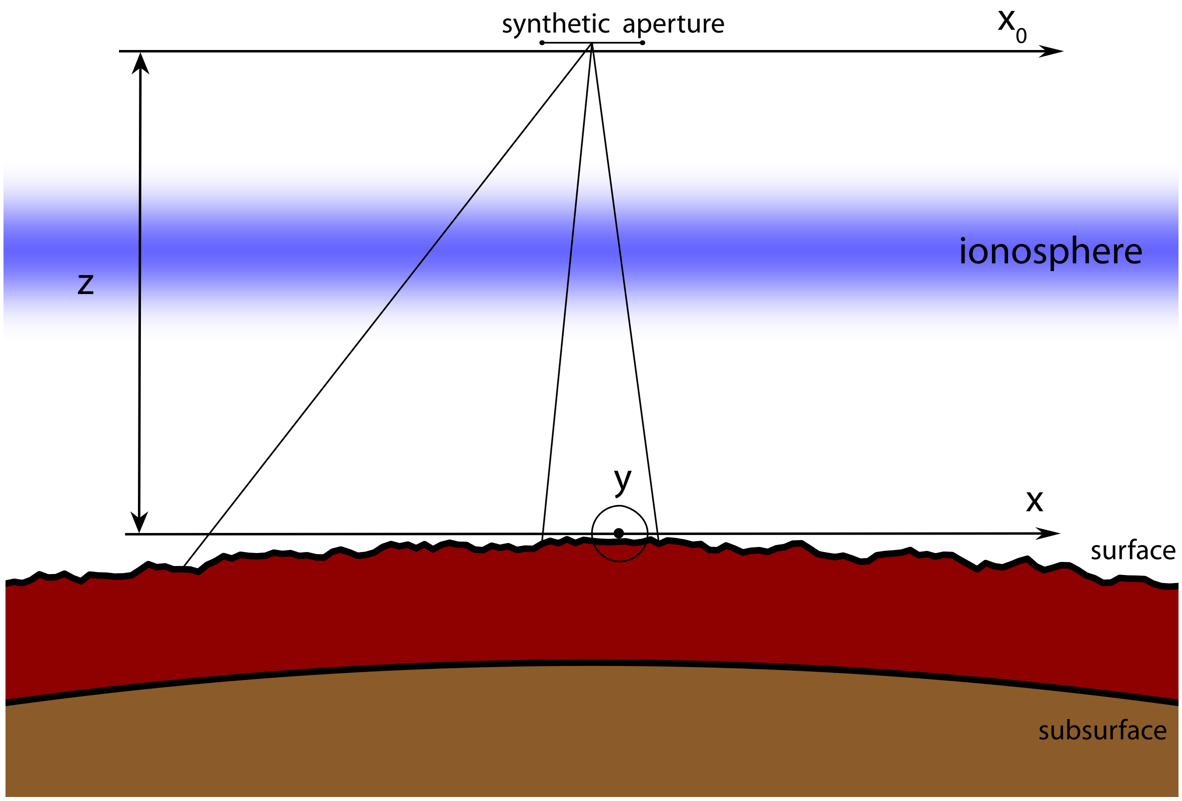

Figure 1. Schematic description of the subsurface radar sounding experiment.

Zienkiewicz, O., R. Taylor, and J. Zhu (Eds.) (2013), *The Finite Element Method: its Basis and Fundamentals (Seventh Edition)*, seventh edition ed., i - pp., Butterworth-Heinemann, Oxford, doi:10.1016/B978-1-85617-633-0.00019-8.

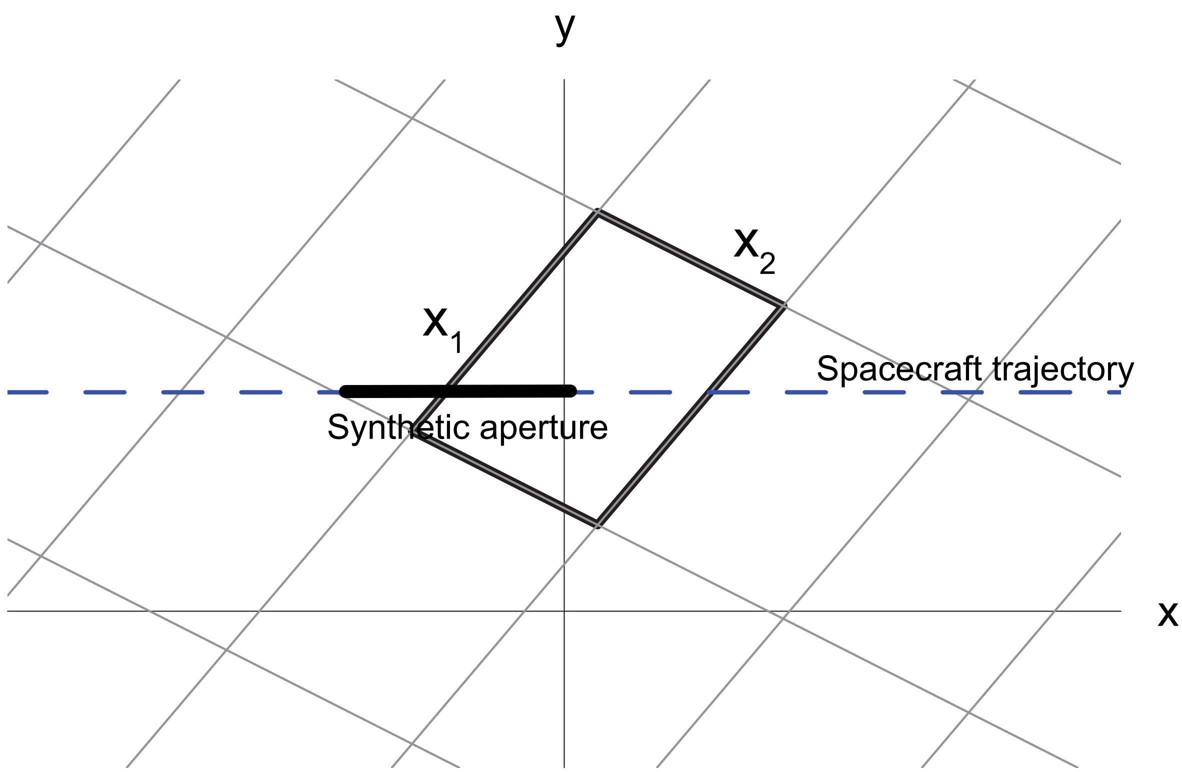

Figure 2. Schematic facet geometry.

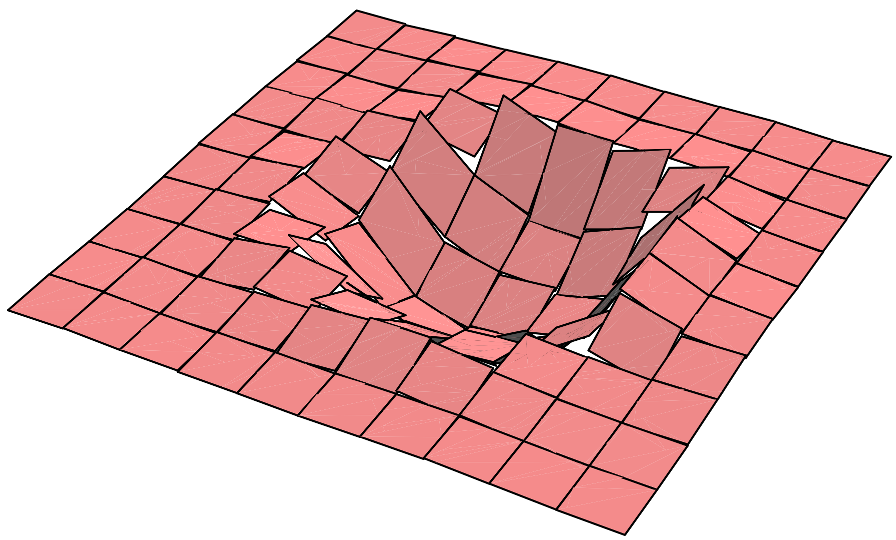

Figure 3. Facet approximation of the planetary surface topography (Martian crater at 22N 61E).

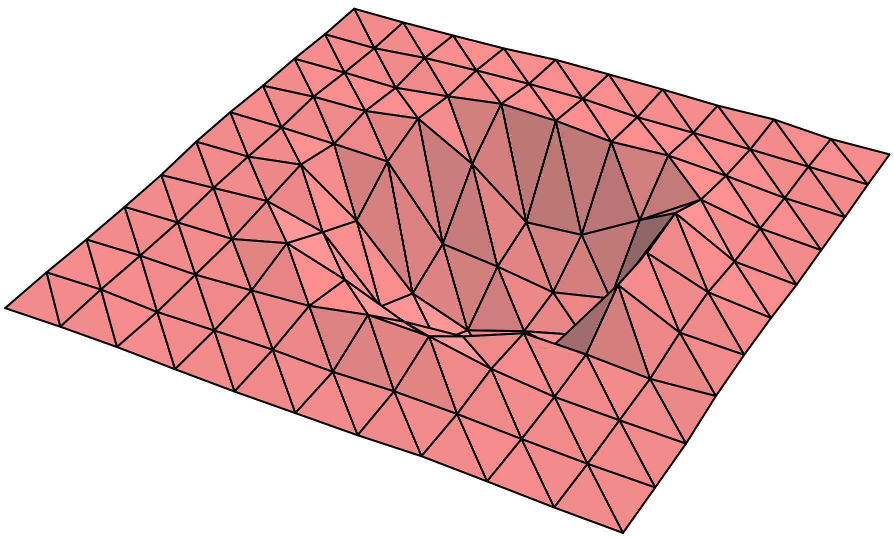

Figure 4. Piecewise-planar triangulation of the planetary surface topography (Martian crater at 22N 61E).

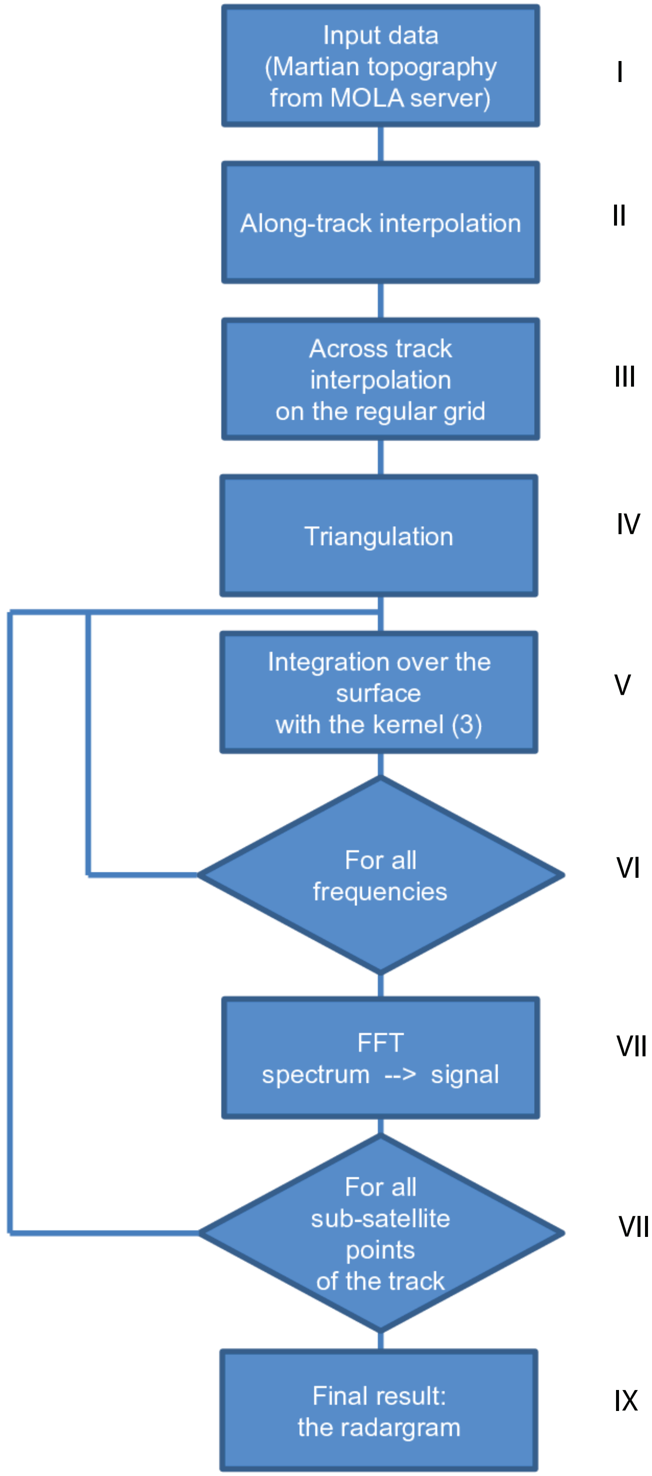

Figure 5. The CLUSIM program flow chart.

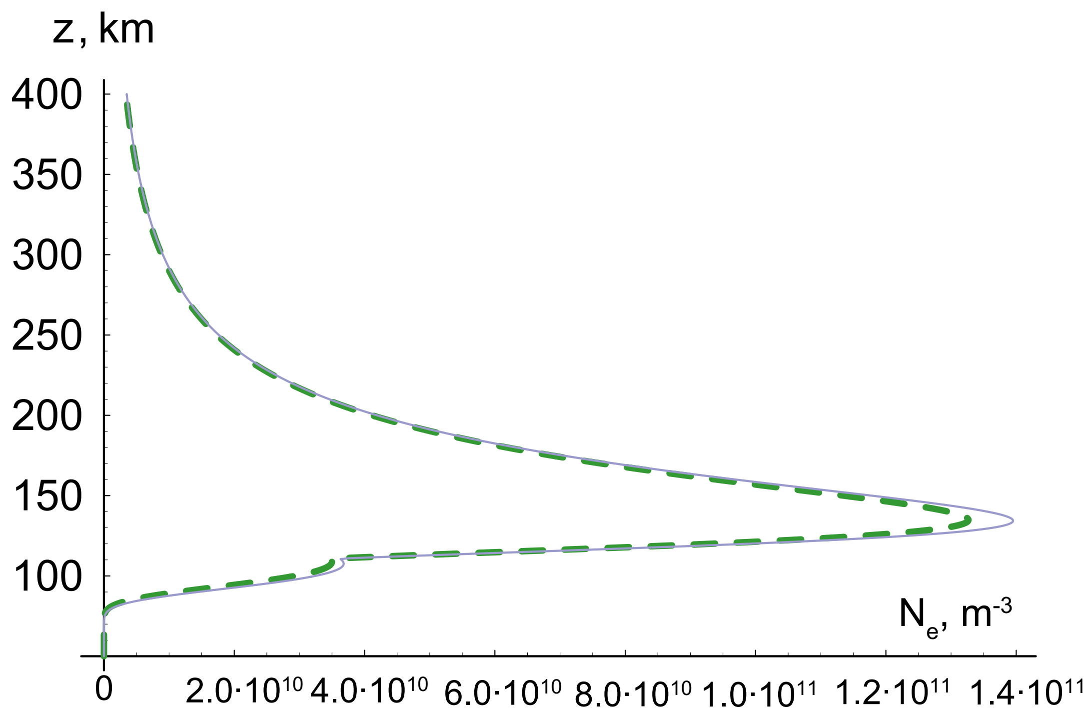

Figure 6. NeMars model ionospheric plasma density profiles for the ending points of satellite orbit portion. Solid line – SZA=61.293, LAT=20.658N, dashed line – SZA=64.95, LAT=26.554N.

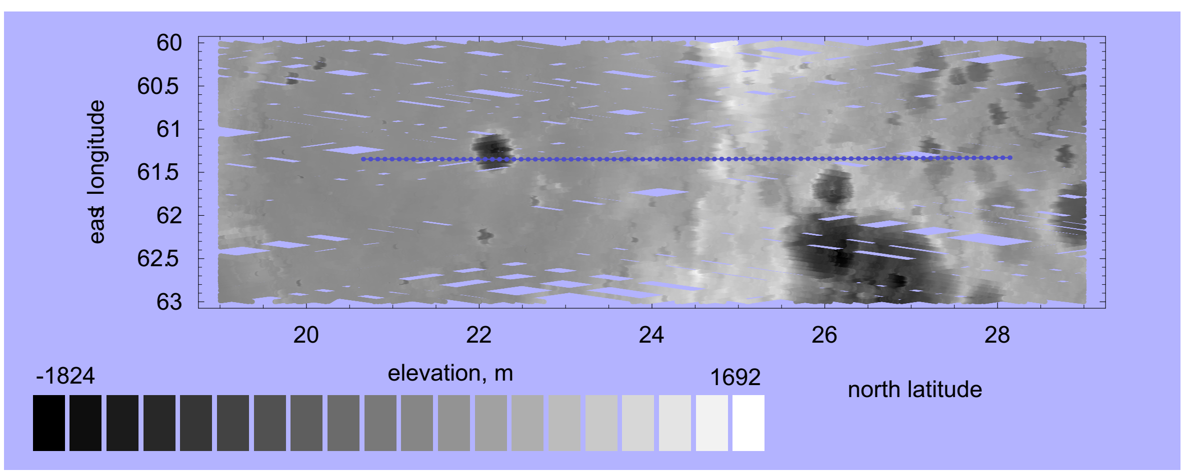

Figure 7. MOLA topography of the martian underlying surface landscape. Blue dotted line - the southmost part of the MEX orbit 9466 subsatellite track.

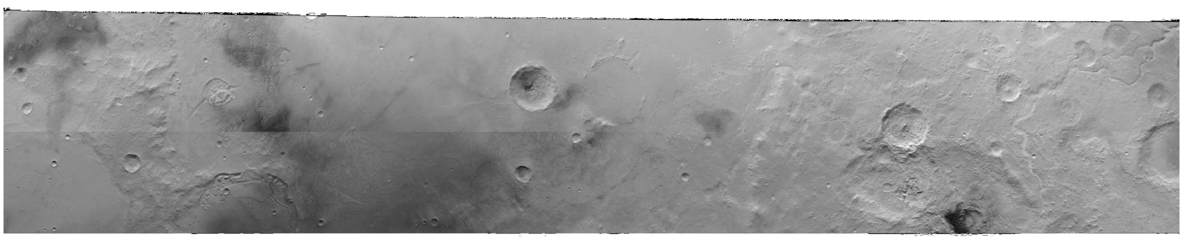

Figure 8. Mosaic of HRSC images H5191_0000_ND3 and H7357_0000_ND3 [*Neukum and Jaumann*, 2004] depicting the subsatellite landscape of the portion of MEX orbit 9466 under investigation. North is the right of the image.

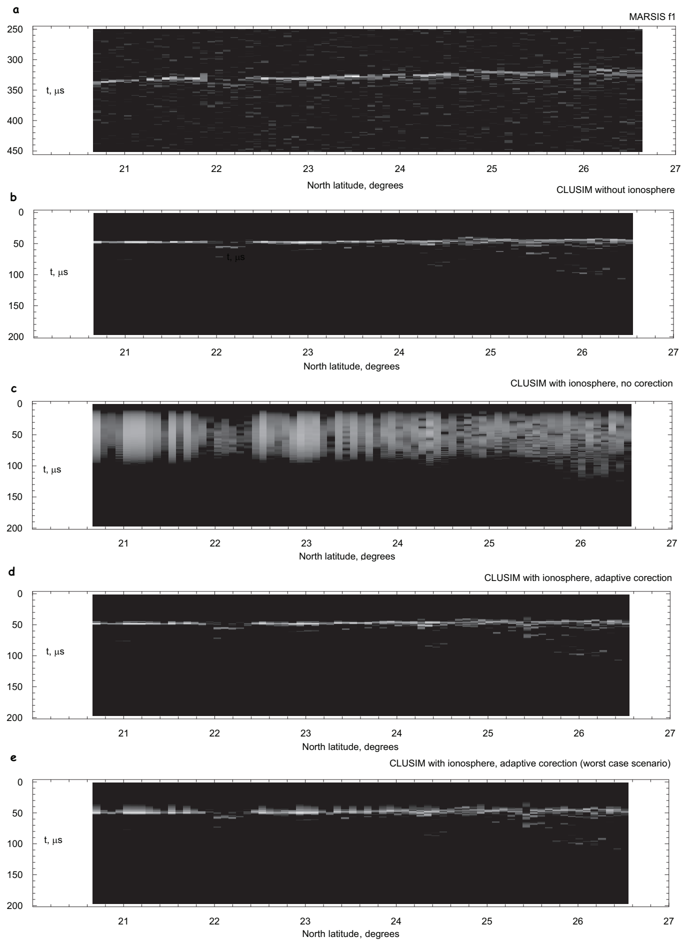

Figure 9. MARSIS radargrams of 9466 MEX orbit. MARSIS Band 4 (4.5 -5.5 MHz). *a* – experimental MARSIS radargram, doppler filter 0, working frequency $f = 5$ MHz (MARSIS band IV), *b* – simulated MARSIS radargram (CLUSIM) without any ionospheric phase shifts, *c* – simulated MARSIS radargram (CLUSIM) with ionospheric phase distortions and no correction, *d* – simulated MARSIS radargram (CLUSIM) with ionospheric phase distortions superimposed and corrected by the maximal contrast adjustment, *e* – simulated MARSIS radargram (CLUSIM) (the same as *e* for the hypothetic "worst case" scenario).

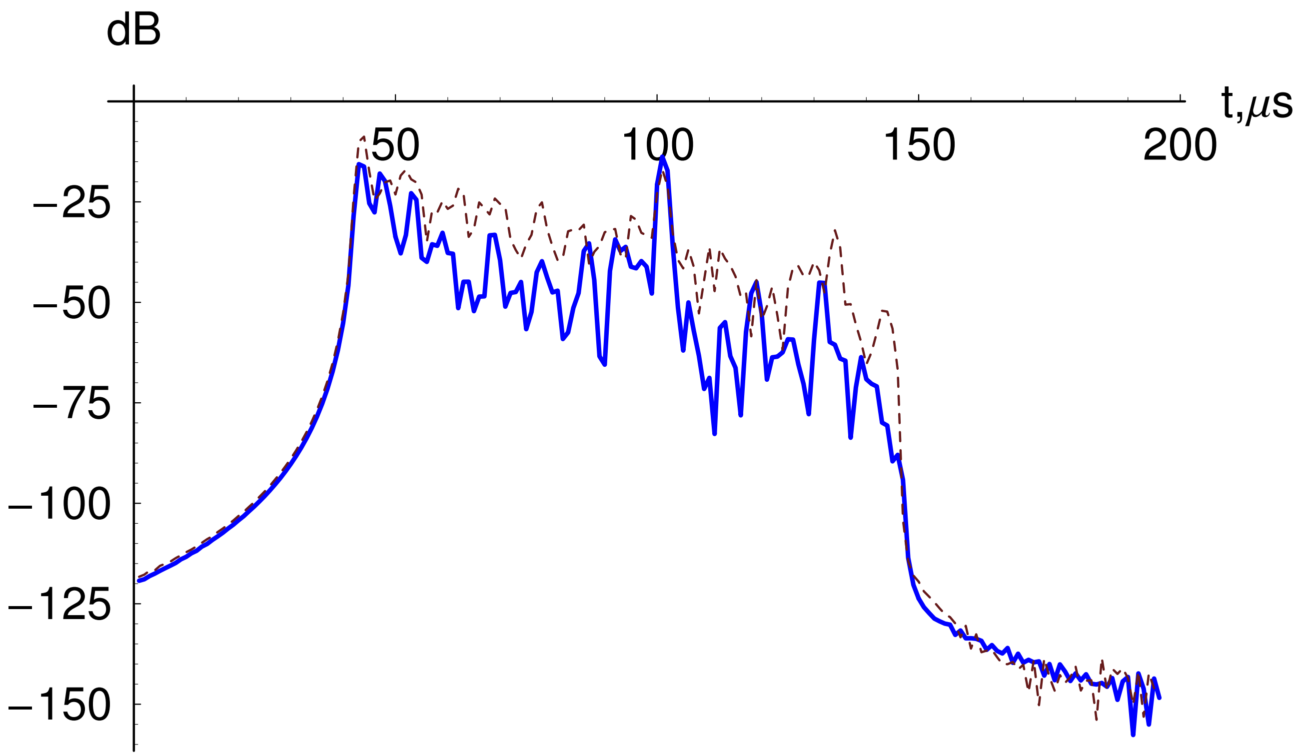

Figure 10. Single pulse MARSIS echo simulation. Solid curve – aperture synthesis is applied (the Doppler filter 0), dotted curve – single pulse echo. Subsatellite point is about $26^{\circ}\,N$ along the 9466 MEX orbit.

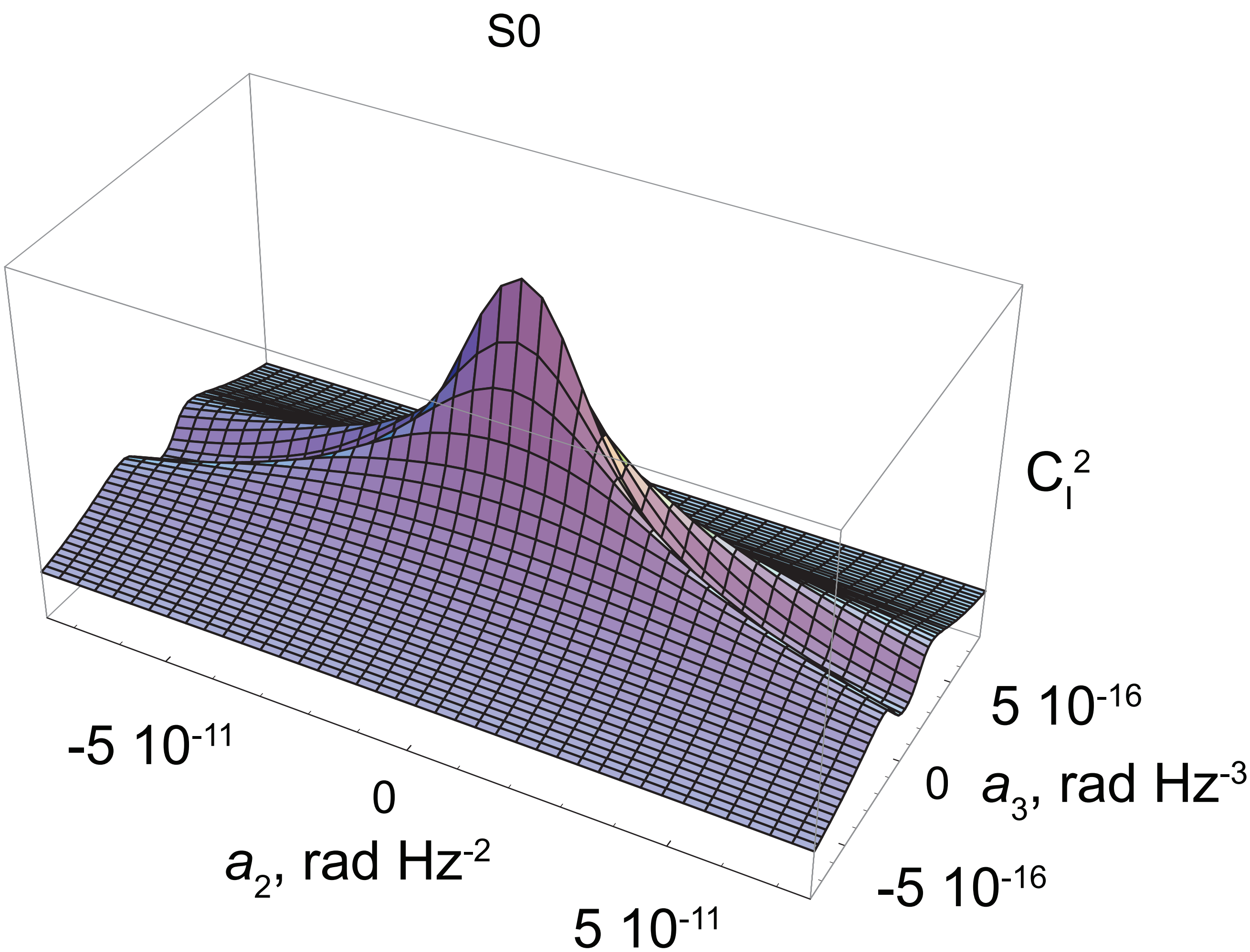

Figure 11. Intensity contrast of the distorted radar reflection from the ideally flat surface (arbitrary units).

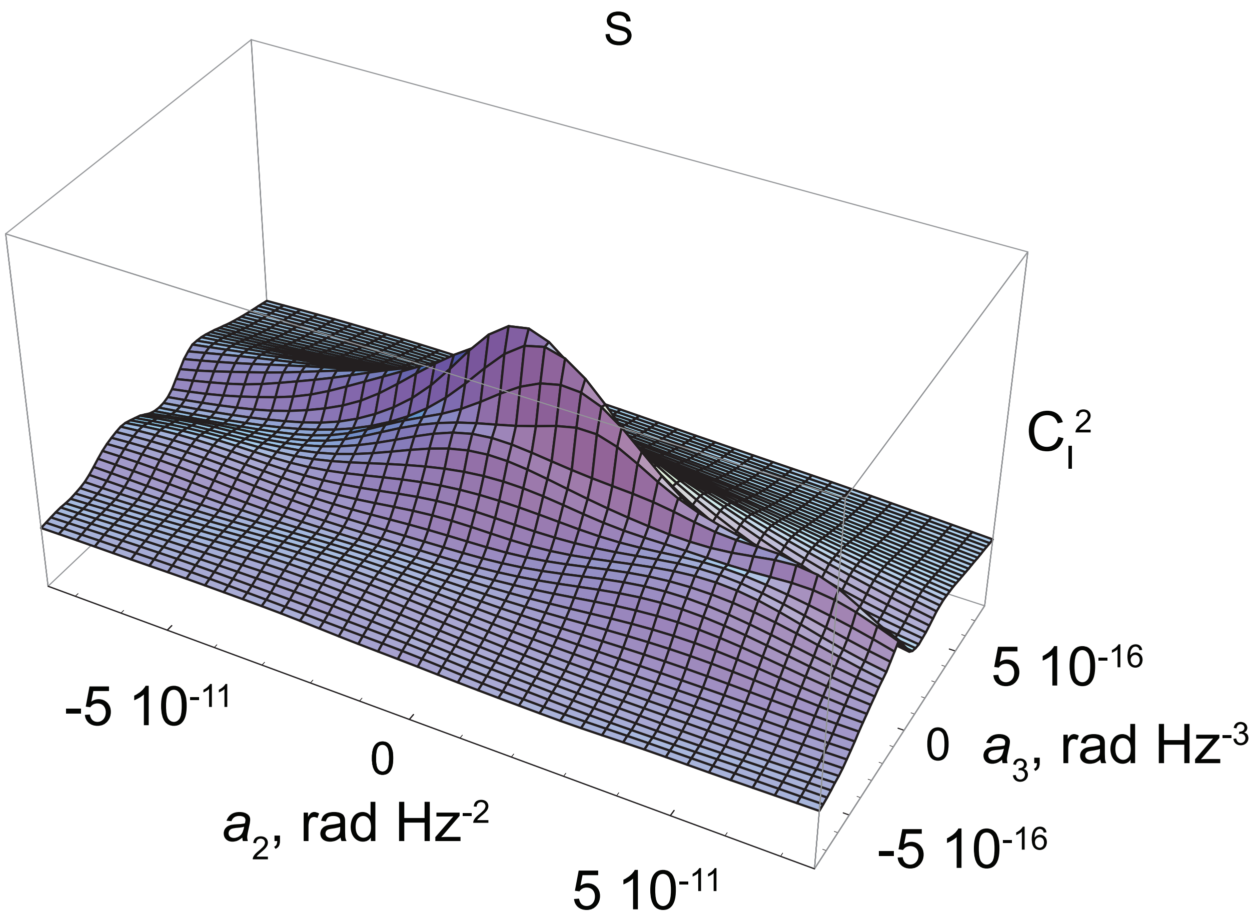

Figure 12. Intensity contrast of the distorted radar reflection from the realistic sufrace terrain (arbitrary units).